Int. J. Heat Mass Transfer. Vol. 34, No. 4/5, pp. 1249–1258, 1991
Printed in Great Britain

0017–9310/91 $3.00 + 0.00

Transient heat and mass transfer in laminar flow forced convection in ducts

E. VAN DEN BULCK
Department of Mechanical Engineering, Katholieke Universiteit Leuven, Celestijnenlaan 300A, B-3030 Heverlee, Belgium

(*Received* 27 *March* 1990 *and in final form* 26 *June* 1990)

Abstract—The modelling of heat and mass regenerators often assumes the heat and mass transfer coefficients to be uniform and constant with time and position within the flow passages of the regenerator. This paper presents a study to examine the validity of this assumption. Experimental breakthrough curves of a single-blow test facility with a desiccant regenerator matrix are examined using a separation technique. The response curves are input to a model which computes the temporal and spatial distributions of the air-side heat and mass transfer coefficients. It is found that the variation of the Nusselt and Sherwood numbers is small for the slower mass transfer waves which determines the performance of regenerative dehumidifiers. The separation technique proves to be a powerful procedure for analysing experimental breakthrough curves.

1. INTRODUCTION

MODELS for regenerative heat exchangers are generally based upon the equations and assumptions as established by the Hausen model [1]. The Hausen equations express the overall energy equation for the adiabatic system {air-stream + heat-exchanger matrix} in combination with a heat transfer equation based upon an overall transfer coefficient, i.e. the transfer rate is proportional to the difference in fluid-mean and matrix-mean temperature. A common assumption in regenerator models is that this overall heat transfer coefficient is constant throughout the exchanger at all times. However, it is known from, e.g. single-blow experiments that there exist non-uniform temperature distributions within the matrix which, due to the periodic nature of regenerator operation, are transient as well [2]. This axial variation of temperature may cause the heat transfer coefficient to change with position and time. Rapley and Webb [3] stated that there is still some uncertainty at present regarding the appropriate boundary conditions for computing the convective Nusselt number in regenerator passages.

Similar conditions arise with modelling regenerative dehumidifiers. These devices use a desiccant material as an intermediate storage medium to exchange water vapour between two air streams. Solid desiccant dehumidifiers are often configured as rotary heat exchangers with desiccant material lining up the walls of the flow passages. Various models have been proposed for these devices, ranging from detailed finite difference models [4] to effectiveness models [5]. These models are all based upon the assumption that the heat and mass transfer coefficients between the air stream and the desiccant material are uniform throughout the regenerator and are constant with time. However, due to the non-uniform distributions of temperature and humidity ratio in the flow passages of the desiccant regenerator, the validity of this assumption may be questionable. No study has yet been presented which examines the validity of assuming constant transfer coefficients in modelling desiccant dehumidifiers.

This article presents a theoretical and experimental study of the variation of the transfer coefficients with time and position in the flow passages of regenerative dehumidifiers. Rather than investigating the axial distributions which exist in regenerators during normal operation, the distributions which originate from single-blow experiments on regenerator matrices are studied. These latter distributions are representative for the actual distributions in well-operated rotating devices because the initial and boundary conditions are almost the same. However, they can be obtained with greater ease and accuracy.

To study the effect of axial variations of heat flux and wall temperature, a Rosen [6] type analysis of regenerators is employed. In this analysis, separate conservation and diffusion rate equations for the fluid stream and the regenerator matrix are used, rather than linear transfer equations using overall transfer coefficients. These two sets of modelling equations are coupled at the walls of the flow passage through the boundary conditions of continuity of temperature and water vapour mass fraction, and heat and mass fluxes. To reduce the computational effort caused by the coupling of this set of equations, a separation technique proposed by Ghezelayagh and Gidaspow [7] is followed. In this technique the solutions of the two sets of modelling equations are separated and the boundary conditions at the interface between the air stream and the walls of the flow passage are obtained from an analysis of a specifically designed set of experiments. The conservation and diffusion equations for

NOMENCLATURE

c_p	humid air thermal capacitance
$c_{p,a}$	dry air thermal capacitance
$c_{p,w}$	water vapour thermal capacitance
D_{aw}	mass diffusivity of water vapour in air
D_h	hydraulic diameter of a flow passage
e	total energy flux
F	dimensionless distribution function
h	air-stream heat transfer coefficient
h_m	air-stream mass transfer coefficient
i	specific enthalpy of humid air stream
i_w	specific enthalpy of water vapour evaluated at the wall
j	diffusion mass flux of water vapour
k	thermal conductivity of humid air stream
L	length of a flow passage
m	total mass flux of water vapour
P	total pressure within the air stream
q	energy flux by conduction
t	temperature
u	local air stream axial velocity
U	average air-stream velocity in a flow passage
v	local air-stream transversal velocity
w	absolute humidity ratio of air, $\omega/(1-\omega)$
x	axial flow coordinate
y	transverse flow coordinate.

Dimensionless groups

Nu	Nusselt number
Re	Reynolds number
Sh	Sherwood number.

Greek symbols

θ	real measuring time
μ	dynamic viscosity of humid air
ρ	humid air-stream density
ω	water vapour mass fraction in air stream, $w/(1+w)$.

Superscript

+	reduced dimensionless variables.

Subscripts

avg	average values
exp	experimental average values
wall	evaluated at the wall
0	evaluated at selected reference conditions.

the fluid stream and the regenerator matrix may thus be solved sequentially rather than simultaneously.

Section 2 describes the model which is used to compute the distributions of the wall conditions and the wall transfer fluxes. The technique of Ghezelayagh and Gidaspow is employed to obtain the axial distributions of the air-side transfer coefficients in terms of selected experimental data. The experimental apparatus and the results from a set of dynamic sorption experiments designed to separate the modelling equations for the air stream and the wall material are discussed in Sections 3 and 4. The analysis of the experimental data is presented in the following section.

2. MODEL FOR TRANSFER COEFFICIENTS

The transfer coefficients for flow of humid air through the passages of rotary dehumidifiers are obtained from a theoretical model in combination with selected experimental data. The model describes the conservation of momentum, energy and mass for the flow of humid air through a parallel plate configuration. The conservation equations are derived from the general equations of change for a multicomponent mixture in terms of the transport fluxes [8]. These general equations are simplified by a limited set of assumptions and order of magnitude estimates of the various terms appearing in the equations. x measures the position in the flow direction and y the transverse position away from the wall. The velocity components in the x- and y-directions are u and v, respectively.

2.1. *Assumptions*

(1) The humid air flows through parallel passages with complete symmetry around the middle axis. Corner effects due to the rectangular geometry are neglected because of the small aspect ratio of the duct.

(2) The flow is two-dimensional. The major velocity component is in the x-direction.

(3) Humid air is a dilute, binary, ideal gaseous solution of water vapour in air. Transport fluxes are described by their conventional expressions.

(4) Local changes of air density, momentum and temperature with respect to time can be neglected with respect to convective changes. Thus, transient terms in the modelling equations for the air stream may be omitted.

(5) Axial diffusion of momentum, heat and mass is neglected.

(6) Changes in potential energy of the gas are neglected.

(7) Radiative heat fluxes are neglected.

An order of magnitude analysis shows that, for the conditions of the experiments reported in this study, the equations of change can be further simplified by neglecting the following terms: buoyancy forces, viscous heating, heating by compression, thermo-

diffusion, pressure diffusion and forced diffusion of water vapour.

The flow is laminar for the range of Reynolds numbers of the experiments. Because axial diffusion in the fluid stream can be neglected in this analysis, there exists an appropriate scaling technique. The conservation equations and the boundary conditions can be expressed in terms of the reduced variables x^+, y^+, u^+ and v^+. These variables are defined as

$$x^+ = \frac{x}{D_h\, Re_0}, \quad y^+ = \frac{y}{D_h}, \quad u^+ = \frac{u}{U}$$

$$\text{and} \quad v^+ = \frac{vD_h\rho_0}{\mu_0} \tag{1}$$

where the reference variables are defined as

$$\rho_0 U = 4\int_0^{1/4} \rho u \, dy^+ \quad \text{and} \quad Re_0 = \frac{UD_h\rho_0}{\mu_0}. \tag{2}$$

2.2. *Equations of change in differential form*

With the assumptions and approximations listed above, the conservation equations which model the flow of air through the test matrix with heat and mass exchange at the wall can be expressed in terms of the transport properties as follows:

continuity equation

$$\frac{\partial \rho u^+}{\partial x^+} + \frac{\partial \rho v^+}{\partial y^+} = 0$$

equation of motion

$$\frac{\rho}{\rho_0}\left(u^+\frac{\partial u^+}{\partial x^+} + v^+\frac{\partial u^+}{\partial y^+}\right) + \frac{1}{\rho_0 U^2}\frac{dP}{dx^+} = \frac{1}{\mu_0}\frac{\partial}{\partial y^+}\left(\mu\frac{\partial u^+}{\partial y^+}\right)$$

diffusion equation

$$\frac{\rho}{\rho_0}\left(u^+\frac{\partial \omega}{\partial x^+} + v^+\frac{\partial \omega}{\partial y^+}\right) = \frac{1}{\mu_0}\frac{\partial}{\partial y^+}\left(\rho D_{aw}\frac{\partial \omega}{\partial y^+}\right)$$

equation of energy

$$\frac{\rho c_p \mu_0}{\rho_0}\left(u^+\frac{\partial t}{\partial x^+} + v^+\frac{\partial t}{\partial y^+}\right) = \frac{\partial}{\partial y^+}\left(k\frac{\partial t}{\partial y^+}\right) + \left[\rho D_{aw}\frac{\partial \omega}{\partial y^+}\right]\left[(c_{p,w} - c_{p,a})\frac{\partial t}{\partial y^+}\right]. \tag{3}$$

This set of conservation and transport equations forms a set of parabolic partial differential equations which describe the variation of t and ω with y^+ and axial position x^+. These equations need to be supplemented with the appropriate boundary conditions.

2.3. *Boundary conditions*

The boundary conditions for the variables u, v, ω and t for integration in the y-direction need to be specified at the wall, $y = 0$, and at the centre of the channel, $y = D_h/4$. The hydraulic diameter is twice the height of the channel.

For all x^+

at $y^+ = 0$:

$$u^+ = 0, \quad v^+ = -\frac{\rho_0 D_{aw}}{\mu_0}\frac{1}{1-\omega}\frac{\partial \omega}{\partial y^+}$$

and

at $y^+ = \frac{1}{4}$:

$$\frac{\partial u^+}{\partial y^+} = 0, \quad v^+ = 0, \quad \frac{\partial \omega}{\partial y^+} = 0, \quad \frac{\partial t}{\partial y^+} = 0. \tag{4}$$

The conventional boundary conditions that specify the property or flux of temperature and humidity at the wall are absent because they are not known in this analysis technique. These boundary conditions are replaced by local integral conditions and matched with experimental data.

2.4. *Equations of change in integral form*

With these boundary conditions, the equations of change can be integrated in the y^+-direction. Upon inserting the integrated continuity equation, the resulting integral conservation equations read as follows:

continuity equation

$$\frac{d}{dx^+}\left[\int_0^{1/4}\frac{\rho}{\rho_0}u^+\,dy^+\right] = -\frac{\rho D_{aw}}{\mu_0}\frac{1}{1-\omega}\frac{\partial \omega}{\partial y^+}\bigg|_{wall}$$

equation of motion

$$\frac{d}{dx^+}\left[\int_0^{1/4}\left(\frac{\rho}{\rho_0}u^+\right)u^+\,dy^+\right] + \frac{1}{4}\frac{1}{\rho_0 U^2}\frac{dP}{dx^+} = -\frac{\mu}{\mu_0}\frac{\partial u^+}{\partial y^+}\bigg|_{wall}$$

diffusion equation

$$\frac{d}{dx^+}\left[\int_0^{1/4}\left(\frac{\rho}{\rho_0}u^+\right)\omega\,dy^+\right] = -\frac{\rho D_{aw}}{\mu_0}\frac{1}{1-\omega}\frac{\partial \omega}{\partial y^+}\bigg|_{wall}$$

equation of energy

$$\frac{d}{dx^+}\left[\int_0^{1/4}\left(\frac{\rho}{\rho_0}u^+\right)i\,dy^+\right] = -\frac{k}{\mu_0}\frac{\partial t}{\partial y^+}\bigg|_{wall} - \frac{\rho D_{aw}}{\mu_0}\frac{i_w}{1-\omega}\frac{\partial \omega}{\partial y^+}\bigg|_{wall}. \tag{5}$$

The equations of change in this form can be integrated with x^+ if the boundary conditions for $\partial t/\partial y^+$ and $\partial \omega/\partial y^+$ at the wall are known. Rather than using the fluxes at the wall, experimental data in an appropriate form are used to facilitate the integration.

2.5. *Integral matching conditions with experimental data*

The integral conditions which complete the set of boundary conditions can be formulated in terms of experimental data.

For all x^+

$$\left.\begin{aligned}\int_0^{1.4}(\rho u^+)\omega\,\mathrm{d}y^+ &= \omega_{\exp}\int_0^{1.4}\rho u^+\,\mathrm{d}y^+\\ \text{and}\\ \int_0^{1.4}(\rho u^+)i\,\mathrm{d}y^+ &= i_{\exp}\int_0^{1.4}\rho u^+\,\mathrm{d}y^+\end{aligned}\right\}\quad(6)$$

where $\omega_{\exp}$ and $i_{\exp}$ are the experimental average values of the water-vapour mass fraction and enthalpy of the humid air stream at position x^+ in the flow direction.

To obtain these experimental values as functions of x^+, either simultaneous measurements would have to be taken at multiple positions inside the flow channel, or flow properties need to be measured at fixed x for repeated experiments with varying mass flow rate as follows from the definition of x^+. This latter approach is significantly easier to perform and forms the idea of the diagnostic technique outlined in this study.

The integral expressions (5) of the conservation and diffusion equations can be expressed in terms of the reduced variable x^+ if and only if the distributions of the mass and energy fluxes at the wall do not include a characteristic length in the flow direction, enforced independently by the response of the duct material. These fluxes are obtained from the match of the conservation and diffusion equations for respectively the air stream and the wall material at the boundary and therefore may include an axial length scale different from the one suggested in equations (1) and (2). The scale of the spatial distributions of temperature and humidity in the air stream is determined by the largest of the characteristic axial length scales involved. In the experiments for this study the wall is composed of individual particles with dimensions ranging from 160 to 300 μm. These particles are isolated from each other and there is negligible axial diffusion of heat or mass through the particles. The axial length scale within the desiccant layer is therefore the particle diameter. The characteristic axial length in the air stream is $D_h\,Re_0$ and ranges from 0.2 to 1 m for the experiments reported in this study. Because this length is much larger than the particle size, this length determines the global spatial distributions of temperature and humidity.

2.6. *Air side heat and mass transfer coefficients*

The problem of determining the air-side heat and mass transfer coefficients is completely posed at this stage of the analysis. The equations of change in differential (3) and integral form (5), in combination with the boundary conditions (4) and the integral matching conditions (6) can be integrated in order to compute the variation of the wall fluxes $\partial t/\partial y^+$ and $\partial\omega/\partial y^+$ with x^+, with the experimental distributions $\omega_{\exp}(x^+)$ and $i_{\exp}(x^+)$ as input. The transfer coefficients are based upon the following conventional definitions:

for the mass transfer coefficient h_m

$$\left.\begin{aligned}\mathbf{j}_{\text{wall}} &= -\rho D_{\text{aw}}\left.\frac{\partial\omega}{\partial y}\right|_{\text{wall}} = h_m(\omega_{\text{wall}}-\omega_{\text{avg}})\\ \text{and similarly for the heat transfer coefficient } h\\ \mathbf{q}_{\text{wall}} &= -k\left.\frac{\partial t}{\partial y}\right|_{\text{wall}} = h(t_{\text{wall}}-t_{\text{avg}})\end{aligned}\right\}\quad(7)$$

in which k and D_{aw} are the thermal conductivity and mass diffusivity of the humid air at the wall. $\mathbf{j}$ is the water vapour diffusion flux at the wall rather than the total mass flux $\mathbf{m}$, and $\mathbf{q}$ is the energy flux by conduction rather than the total energy flux $\mathbf{e}$. These fluxes are related by

$$\left.\begin{aligned}\mathbf{m}_{\text{wall}} &= \frac{\mathbf{j}_{\text{wall}}}{1-\omega}\\ \mathbf{e}_{\text{wall}} &= \mathbf{q}_{\text{wall}}+i_{\text{w}}\mathbf{m}_{\text{wall}}.\end{aligned}\right\}\quad(8)$$

The Nusselt and Sherwood numbers are defined conventionally as

$$Nu = \frac{hD_h}{k}\quad\text{and}\quad Sh = \frac{h_mD_h}{\rho D_{\text{w}}}.\quad(9)$$

3. EXPERIMENTAL APPARATUS

The experimental results which are required in this study relate to the transient exchange of momentum, heat and mass in laminar flow of humid air through parallel plates with desiccant-coated surfaces in single-blow experiments. Ghezelayagh and Gidaspow [7], Biswas *et al.* [9], Clark *et al.* [10], Allander [11] and Pesaran and Zangrando [12] described single-blow apparatuses and desiccant matrices which facilitate this type of experiment. The experimental procedure involves a common sequence of operations. A humid air stream with controlled properties and mass flow rate is passed through the flow passages of a desiccant matrix at fixed inlet conditions. Initial conditions for the matrix are established when the desiccant matrix is in equilibrium with the air stream. A sudden change in the air inlet conditions is then introduced and the air outlet state is recorded with time. This response of the air-stream outlet state forms the experimental data that characterize the exchange performance of the test matrix and which are the subject of the discussion presented in this paper.

The test matrix is arranged as a vertical stack of 74 parallel rectangular passages with hydraulic diameter $D_h = 2.0\pm6\%$ mm. Each passage has a width of $126\pm0.9\%$ mm, and a flow length $L = 0.203\pm0.2\%$ m. The walls of the flow passages are coated with crushed, regular-density silica gel particles with a diameter of 0.177–0.297 mm, yielding a total mass

of dry desiccant of $0.49 \pm 3\%$ kg. The total internal transfer area is $3.65 \pm 4.5\%$ m^2 and the free flow area is $0.00927 \pm 3\%$ m^2. The $\pm$ values in these and the following statements denote uncertainties.

Temperature, humidity and pressure sensors are provided at the entrance and exit faces of the test matrix. The temperature of the air stream is measured using copper–constantan thermocouples, with a total error of less than ± 0.2°C for the configuration and conditions reported in this study. The humidity of the process air stream is measured through sampling with chilled-mirror, dewpoint hygrometers. The error in absolute humidity due to errors in the measurement of the dewpoint temperature and ambient pressure is about 1.5% for humidity differences and 2.8% for absolute humidity measurements. Pressure drops across the test matrix are measured with electronic capacitive transducers, with an accuracy of $\pm 0.5\%$. The measurement of the air flow rate is done by means of an orifice plate inserted in a circular cross-section conduit ahead of the test section, giving an accuracy of $\pm 2.5\%$. Pressure drop and flow rate measurements were checked for consistency and the friction factor vs Reynolds number follows the theoretical correlation for laminar flow through parallel plates.

A full description of the single-blow experimental apparatus is given in ref. [13] and the test procedures are described in ref. [14].

4. EXPERIMENTAL RESULTS

The integral matching conditions (6) in the model for computing the heat and mass transfer coefficients require experimental distributions of air-stream temperature and humidity with position in the flow direction x^+. These distributions are retrieved from single-blow experiments with simultaneous heat and mass transfer. The breakthrough curves obtained from single-blow experiments on heat exchangers are different if mass exchange is occurring simultaneously. For heat exchangers, the thermal wave is an expansion wave, continuously spreading as it progresses through the exchanger passages. The shape of this wave never becomes *fully developed* and therefore depends at all times on its initial shape; that is, the change of the inlet conditions with time. Distributions of this type for linear systems are modelled by the Anzelius [15] or Schumann [16] equations.

The breakthrough curves encountered in single-blow experiments involving adiabatic mass transfer are associated with the propagation of two confined, spatial property distributions: air-stream temperature and humidity. Ruthven discussed in detail the propagation and dispersion of these distributions, also called waves [17]. There exists a thermal wave, during which most of the sensible energy is exchanged between the air stream and the matrix, and a mass transfer wave which incorporates the majority of the mass exchange. The thermal wave is narrow and propagates at high speed through the matrix, whereas the mass transfer wave is wider and slower. The respective wave speeds are proportional to the ratio of thermal and mass capacitances of the fluid stream and matrix. The two distributions are usually completely separated, with a well-defined intermediate state in between the two transfer zones.

4.1. *Constant pattern breakthrough curves*

With mass transfer, the nonlinearity of the equilibrium sorption isotherm may introduce favourable wave patterns which are not encountered in heat transfer. For selected matrix-initial and fluid-inlet states, the property distributions can be *constant-pattern waves*, i.e. the shape of the distributions is preserved as the waves progress through the matrix. For the system regular-density silica gel and humid air, theoretical analyses in ref. [5] and experimentally verified in ref. [18] show that constant pattern waves occur during regeneration of the wet desiccant with a hot air stream. This process is a desorption process as opposed to an adsorption process where a humid air stream is dried by the regenerated desiccant.

Constant pattern waves become rapidly fully established after they originate at the inlet face of the matrix. The shape and width of the mass transfer wave in desorption processes are constant, and, for reasonable-quality inlet steps and sufficiently long bed lengths, are independent of the sharpness of the step change in inlet conditions. Furthermore, the wave dispersion is well defined and independent of the air-stream mass flow rate.

4.2. *Experimental results*

A series of 14 constant-pattern desorption experiments have been performed. The temperature and water content of the desiccant matrix are initialized at selected conditions, and a step change in the inlet temperature of the air stream is introduced. As stated previously, the step change does not need to be square for generating repeatable breakthrough curves because of the constant-pattern condition. The air-stream mass flow rate is varied in a systematic sequence starting from 0.013 to $0.028 \pm 2.5\%$ kg s^{-1}. Each experiment has the same pair of matrix-initial and air-inlet conditions, respectively ($t_0 = 29.6 \pm 0.8$°C, $\omega_0 = 0.0141 \pm 0.0006$ kg kg^{-1}) and ($t_2 = 67.1 \pm 0.2$°C, $\omega_2 = 0.0157 \pm 0.0004$ kg kg^{-1}). For these conditions, the thermal and mass transfer waves are fully separated, and the experimental intermediate state properties are ($t_1 = 37.1 \pm 0.3$°C, $\omega_1 = 0.0227 \pm 0.0004$ kg kg^{-1}). The Reynolds number Re based upon the fluid inlet state properties ranges from 140 to 425 for these experiments, providing a passage flow well in the laminar regime.

The experimental results are presented as graphs showing the air-stream outlet conditions, i.e. temperature and humidity ratio, vs the dimensionless flow length x^+ defined for each of the experiments as

$$x^+ = \frac{L}{D_h \overline{Re}}.$$

This dimensionless flow length or Graetz variable x^+ ranges from 0.23 to 0.70 with steps of 0.05 for the alternate experiments. The constant pattern condition allows the measured fluid outlet property responses with time to be interpreted as the temporal distributions with position in the flow direction x^+. The analysis presented here focuses on the mass transfer wave of the desorption experiments because the property distributions associated with this wave are constant pattern waves and experimentally well defined.

4.3. *Curve-fit*

Figures 1(a) and (b) show the experimental air-stream outlet conditions for each of the 14 values of x^+ with the real measuring time θ as a parameter. The conditions on the left of Figs. 1(a) and (b) are those of the inlet state (t_2, ω_2), and the conditions on the right are the intermediate state properties (t_1, ω_1). Fourteen discrete experimental data points are available to represent the distributions. The experimental distributions $\omega_{exp}(x^+)$ and $t_{exp}(x^+)$ in equations (6) need to be represented by continuous smooth functions of x^+. Thus an interpolating curve-fit of the experimental data points has to be established.

Using least-square curve-fitting techniques with cubic splines and optimized knot location, the experimental distributions for the six values of the sampling time θ in Figs. 1(a) and (b) can be shifted to the left over a distance x_0 proportional with θ to overlap with a single distribution curve. This shift is linear with the constant wave speed and can be determined from the experimental distributions in Figs. 1(a) and (b) with high accuracy. The shifted experimental distributions are shown in Figs. 2(a) and (b) and are centred about the point of maximum slope of the curves. The r.m.s. scatter of the experimental data about this 'best' fit is 0.34°C for temperature and 0.00012 kg kg^{-1} for humidity. These values are of the order of the accuracy of the measurements, and therefore show that the distributions satisfy the constant-pattern condition. Although this condition is not necessary for the analysis, it provides redundancy in the measurement of the experimental breakthrough curves and thus increases the accuracy of the curve-fit.

For input to the model equations, the experimental distributions need to be represented by a continuous curve-fit with smooth derivatives up to high order, as

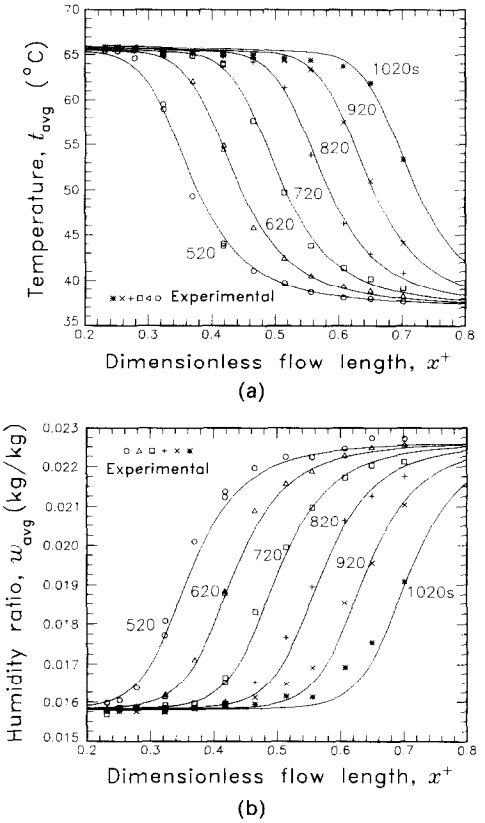

FIG. 1. (a) Experimental distributions of average air-stream temperature t_{avg} with the dimensionless flow length x^+ in comparison with the F curve-fit and with measuring time θ as parameter. (b) Experimental distributions of average air-stream humidity ratio w_{avg} with the dimensionless flow length x^+ in comparison with the F curve-fit and with measuring time θ as parameter.

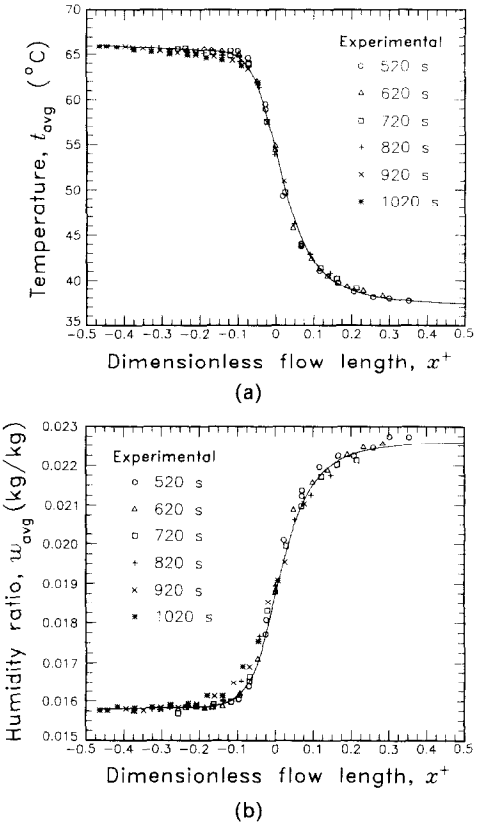

FIG. 2. (a) Shifted experimental distributions of air-stream temperature t_{avg} with the dimensionless flow length x^+ in comparison with the F curve-fit and with measuring time θ as parameter. (b) Shifted experimental distributions of air-stream humidity ratio w_{avg} with the dimensionless flow length x^+ in comparison with the F curve-fit and with measuring time θ as parameter.

is explained in the next section. Such a curve-fit can be obtained with the following normalized distribution. Define $F(x; p, q)$ as the solution of the initial value problem

$$\frac{dF}{dx} = \frac{[(1+F)+\sqrt{((1+F)^2+\varepsilon^2)}]^p \times [(1-F)+\sqrt{((1-F)^2+\varepsilon^2)}]^q}{dF/dx|_{x=0}} \quad (10)$$

with ε small, say 0.01, and with an initial condition at $x = 0$

$$F(0; p, q) = \frac{p-q}{p+q}.$$

This function F is continuous and has an infinite number of smooth continuous derivatives for all x. The parameters p and q are shape parameters which determine the skewness of F and the tendency of the distribution to tail off at $F = \pm 1$. For $p = q = 1$, F approximates a symmetrical Gaussian distribution and F has the shape of the error function.

The experimental distributions $\omega_{exp}(x^+)$ and $t_{exp}(x^+)$ can each be least-square curve-fitted with the cubic splines and also with the F function and appropriate scaling parameters with an accuracy as good as a cubic spline fit with optimized knot locations.

5. ANALYSIS

Conventional second-order finite difference solutions of the system of continuity and momentum equations (3) give fluctuations in the velocity and pressure terms. Rather than using difference algorithms specifically developed to smooth these fluctuations, such as upwind differencing, the method of orthogonal collocation with cubic Hermite splining over finite elements is used for this analysis. This method inherently gives smooth profiles for the velocities and fluxes. Also the nonlinearity of the momentum-convection terms and the change of thermophysical properties with temperature and water vapour mass fraction is included without the need for iteration. The integral form (5) of the conservation equations gives increased accuracy for the numerical solution and can be incorporated without adding to the complexity or computation time of the solution.

The algorithm for the method of orthogonal collocation for solving one-dimensional, parabolic partial differential equations is described in detail by Lapidus and Pinder [19]. In essence, this method approximates the various profiles in the y-direction of the velocity u, temperature t, and water vapour mass fraction ω, with splines of cubic Hermite polynomials defined over a sequence of finite elements. With this representation the partial differential equations (3), expressed at the Gaussian quadrature points within each element, are reduced to a system of ordinary differential equations in the nodal variables representing u, t, ω and P. The integral equations (5) are reduced similarly to ordinary differential equations. The boundary conditions (4) and (6) are reduced to a set of linear algebraic equations in the nodal variables. This system of mixed equations can be integrated with x^+ with a conventional ODE solver to yield the axial distributions of temperature and humidity within the air stream, $t(x^+, y^+)$ and $\omega(x^+, y^+)$. Both Nu and Sh are obtained from equations (7) and (9).

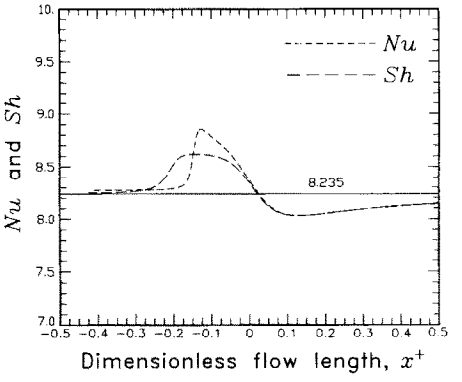

FIG. 3. Air Nusselt and Sherwood number distributions with the dimensionless flow length x^+ for the F curve-fit.

In this analysis, five finite elements are used in combination with the fourth-order Runge–Kutta method. The experimental data in the integral boundary conditions obtained from the previous section are inserted in equations (6). Solutions are obtained and presented for both the cubic spline and the F curve-fit distribution function representing the experimental data. The initial flow conditions are those of fully developed Hagen–Poiseuille flow through parallel plates with uniform temperature and humidity. The thermophysical properties, ρ, c_p, μ, k, D_{aw}, are obtained from the most recent published standards for property evaluation for air–water vapour mixtures [18].

Figures 3 and 4 show the distributions in the x^+-direction of, respectively, the air-side Nusselt and Sherwood numbers, and the conductive and total energy and mass diffusion fluxes as computed by solv-

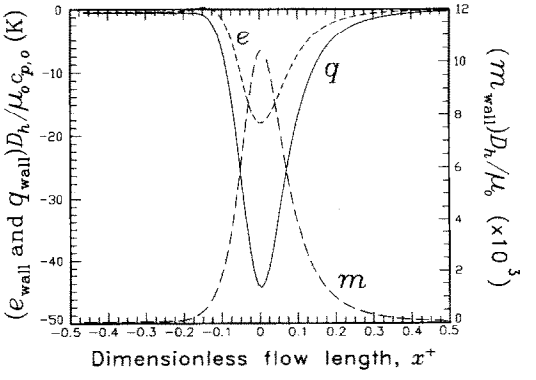

FIG. 4. Air mass and energy flux distributions with the dimensionless flow length for the F curve-fit.

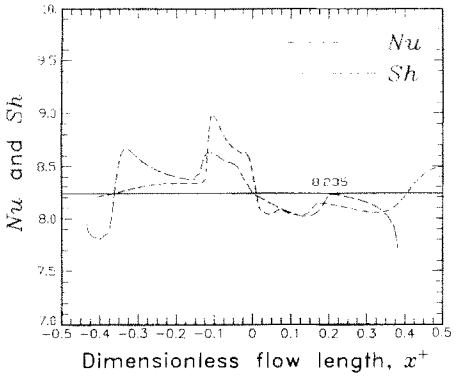

FIG. 5. Air Nusselt and Sherwood number distributions with the dimensionless flow length for the cubic spline curve-fit.

ing the modelling equations (3)–(6) in combination with the F curve-fit. The variation of the local Nusselt and Sherwood numbers is due to the non-uniform distributions of the wall fluxes. These flux distributions have the shape of a skewed Gaussian distribution, as shown in Fig. 4. The fluxes are constant in the region $x^+ < -0.3$ prior to the start of the wave. In this region the computed Nu and Sh agree with the asymptotic value for constant fluxes, 8.235 [20], as indicated in Fig. 3 and this agreement substantiates the accuracy of the numerical model. The Sherwood number starts to increase at $x^+ \approx -0.3$, and the Nusselt number increases at $x^+ \approx -0.2$ in Fig. 3. This difference is due to the sensitivity of the Nusselt and Sherwood numbers to the representation of the experimental data with interpolating functions.

Figure 5 shows the Nu and Sh distributions for the cubic spline curve-fit. These latter figures illustrate the effect of the curve-fit representation on the results of the calculations. The local Nusselt and Sherwood numbers depend mainly on the distributions of the *derivatives* of the wall fluxes, and the discontinuity of the third derivative of the cubic splines at the knots has a major effect on the computed transfer coefficients. This result shows that the experimental data for input to the analysis need to be represented with a curve-fit which is smooth and has continuous, smooth derivatives up to at least second order. These requirements are met by the integrated F distribution as introduced in equation (10). Furthermore, the second derivative of the curve-fit should approximate the second derivative of the experimental temperature and humidity distributions with good accuracy. Such a curve-fit requires extremely accurate measurements of the air-stream temperature, humidity and mass flow rate, and a large series of highly repeatable experiments for a wide range of the air-stream mass flow rate. These conditions are partly met by the redundancy of the constant-pattern breakthrough curves.

The variations of Nu and Sh with position are important in the window $-0.2 \leqslant x^+ \leqslant 0.2$ where the magnitudes of the mass and energy transfer fluxes are largest. In this region, Fig. 3 indicates that the variations of Nu and Sh about the average value are similar and small, about $\pm 5\%$. The average numbers compare with the solution for a constant heat or mass flux, 8.235. To check these results, the computed distributions can be compared with theoretical distributions obtained from an analogy theory. Graber showed that the Nusselt number for forced convection, laminar flow in ducts depends on the derivative of the heat flux [21]. For an exponential distribution of the local wall heat flux, the temperature profile is fully developed, the Nusselt number is constant and, for flow through parallel plates, can be approximated with the following linear equation:

$$Nu = 8.235 + 0.0222 \frac{1}{\mathbf{q}} \frac{d\mathbf{q}}{dx^+}. \tag{11}$$

For non-exponential flux distributions, the temperature profile is continuously developing. However, it may be expected that the local Nusselt number can still be approximated by equation (11). The local wall heat flux is proportional to the derivative of the average fluid temperature with respect to x^+, and, in this study, can be directly obtained from the F curve-fit of the experimental data. The estimated distributions of the Nusselt and Sherwood numbers computed with equation (11) are compared with the complete solution of the conservation equations in Fig. 6. The Sherwood number is computed by replacing $\mathbf{q}$ with $\mathbf{j}$ in equation (11). The respective profiles do not exactly overlap because the local wall fluxes do not vary exponentially with x^+, and the local temperature and humidity profiles are continuously developing. However, the corresponding curves show the same variation and that fact substantiates the results of this analysis.

Graber's analysis can be used to estimate the variation of the air-side transfer coefficients during adsorption. The distributions associated with adsorption are generally expansion waves [17]. These distributions are more smeared out than constant-pattern waves and therefore the axial variation of the

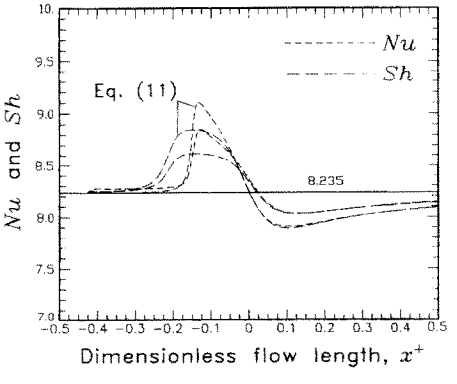

FIG. 6. Air Nusselt and Sherwood number distributions with the dimensionless flow length for the F curve-fit in comparison with Graber's analysis.

transfer coefficients may be even smaller for adsorption than for desorption.

6. CONCLUSION

The axial distribution of the air-side heat and mass transfer coefficients occurring in regenerative dehumidifiers is evaluated from experimental breakthrough curves obtained from single-blow experiments. It is shown that the heat and mass transfer coefficients vary little with position in the flow direction for the slowly moving mass transfer wave. This result validates the assumption of constant transfer coefficients in the modelling of rotary dehumidifiers.

The technique which is used to compute the distributions was introduced by Ghezelayagh and Gidaspow for isothermal mass transfer. This study extends the use of this technique to simultaneous heat and mass transfer occurring in desiccant regenerators. It is shown that this technique can provide a powerful procedure for analysing experimental breakthrough curves.

The variation of the transfer coefficients due to axially varying wall fluxes can also be examined by Graber's analysis. His correlation shows that the variation of the local Nusselt number is proportional with the first derivative of the logarithm of the wall heat flux with respect to position in the flow direction. Curve-fits of experimental breakthrough curves therefore need to be continuous and smooth up to a high order of differentiation. A distribution function for curve-fitting which satisfies these requirements is presented in equation (10).

Acknowledgements—The author wishes to thank the staff of the Solar Energy Laboratory of the University of Wisconsin–Madison for the financial support and their advice during his extended stay there. The author also wishes to thank the Solar Energy Research Institute in Golden, Colorado, for making their experimental facilities available.

REFERENCES

1. R. K. Shah, Thermal design theory for regenerators. In *Heat Exchangers, Thermal–Hydraulic Fundamentals and Design* (Edited by S. Kakac, A. E. Bergles and F. Mayinger), pp. 721–763. Hemisphere, Washington, DC (1981).
2. W. M. Kays and A. L. London, *Compact Heat Exchangers* (3th Edn), pp. 79–101. McGraw-Hill, New York (1984).
3. C. W. Rapley and A. I. C. Webb, Heat transfer performance of ceramic regenerator matrices with sine-duct shaped passages, *Int. J. Heat Mass Transfer* **26,** 805–814 (1983).
4. I. L. Maclaine-cross, A theory of combined heat and mass transfer in regenerators, Ph.D. Thesis, Monash University, Australia (1974).
5. E. Van den Bulck, J. W. Mitchell and S. A. Klein, Design theory for rotary heat and mass exchangers, *Int. J. Heat Mass Transfer* **28,** 1575 1595 (1985).
6. J. B. Rosen, General numerical solution for solid diffusion in fixed beds, *Ind. Engng Chem.* **46,** 1590–1594 (1954).
7. H. Ghezelayagh and D. Gidaspow, Micro–macropore model for sorption of water on silica gel in a dehumidifier, *Chem. Engng Sci.* **37,** 1181–1197 (1982).
8. R. B. Bird, W. E. Stewart and E. N. Lightfoot, *Transport Phenomena*. Wiley, New York (1960).
9. P. Biswas, S. Kim and A. F. Mills, A compact low-pressure drop desiccant bed for solar air conditioning applications: analysis and design, *J. Solar Energy Engng* **106,** 153–158 (1984).
10. J. E. Clark, A. F. Mills and H. Buchberg, Design and testing of thin adiabatic desiccant beds for solar air conditioning applications, *J. Solar Energy Engng* **103,** 89–91 (1981).
11. C. G. Allander, Untersuchung des adsorptionsvorganges in adsorbentenschichten mit linearer adsorptionsisotherme, *K. Tek. Hoegsk. Handl.* **70,** 1–160 (1953).
12. A. A. Pesaran and F. Zangrando, Isothermal dehumidification of air in a parallel passage configuration, ASME Paper 85-HT-72, 23rd ASME/AIChE Natn. Heat Transfer Conf. (1985).
13. A. A. Pesaran, I. L. Maclaine-cross and E. Van den Bulck, Measurements on promising dehumidifier materials and geometries, SERI/TR-252-2898, Solar Energy Research Institute, Golden, Colorado (1986).
14. E. Van den Bulck and S. A. Klein, A single-blow test procedure for compact heat and mass exchangers, *J. Heat Transfer* **112,** 317–322 (1990).
15. A. Anzelius, Uber Erwarmung vermittels durchstromender Medien, *Z. Angew. Math. Mech.* **6,** 291–294 (1926).
16. T. E. W. Schumann, Heat transfer: a liquid flowing through a porous prism, *J. Franklin Inst.* **208,** 405–416 (1929).
17. D. M. Ruthven, *Principles of Adsorption and Adsorption Processes*, pp. 124–166. Wiley, New York (1984).
18. E. Van den Bulck, Convective heat and mass transfer in compact regenerative dehumidifiers, Ph.D. Thesis, University of Wisconsin–Madison, Madison, Wisconsin (1987).
19. L. Lapidus and G. F. Pinder, *Numerical Solution of Partial Differential Equations in Science and Engineering*. Wiley, New York (1982).
20. R. K. Shah and A. L. London, Laminar flow forced convection in ducts. In *Advances in Heat Transfer* (Edited by F. I. Thomson and J. P. Hartnett), Suppl. 1. Academic Press, New York (1978).
21. H. Graber, Der Warmeubergang in glatten Rohren zwischen parallelen Platten, in Ringspalten und langs Rohrbundeln bei exponentieller Warmeflussverteiling in erzwungener laminarer oder turbulenter Stromung, *Int. J. Heat Mass Transfer* **13,** 1645–1703 (1970).

TRANSFERT VARIABLE DE CHALEUR ET DE MASSE EN CONVECTION FORCEE LAMINAIRE DANS LES TUBES

Résumé—La modélisation des régénérateurs de chaleur et de masse suppose souvent que les coefficients de transfert de chaleur et de masse sont uniformes et constants avec le temps et la position dans les passages de l'écoulement. On présente une étude pour examiner la validité de cette hypothèse. Des courbes expérimentales avec un montage à un seul courant et une matrice de régénérateur d'un produit déshydratant sont examinés en utilisant une technique de séparation. Les courbes de réponse sont entrées dans un modèle qui calcule les distributions temporelles et spatiales des coefficients de transfert de chaleur et de masse du côté air. On trouve que la variation des nombres de Nusselt et de Sherwood est faible pour les cycles les plus lents de transfert de masse qui déterminent les performances des deshumidificateurs régénérateurs. La technique de séparation peut être une procédure puissante pour analyser les courbes expérimentales.

INSTATIONÄRER WÄRME- UND STOFFTRANSPORT BEI LAMINARER ERZWUNGENER KANALSTRÖMUNG

Zusammenfassung—Bei der Beschreibung der Vorgänge bei Wärme- und Stoffrückgewinnung wird oft von einheitlichen, zeit- und ortsunabhängigen Wärme- und Stoffübergangskoeffizienten innerhalb der Strömung ausgegangen. In der vorliegenden Arbeit wird untersucht, inwieweit diese Annahme gerechtfertigt ist. Unter Verwendung eines Separationsverfahrens werden experimentell ermittelte Ausgleichskurven für eine eingängige Versuchsanordnung mit einer Entfeuchtungskomponente untersucht. Die resultierenden Kurven dienen als Eingabedaten für ein Modell, mit dem die zeitlichen und örtlichen Verteilungen der luftseitigen Wärme- und Stoffübergangskoeffizienten berechnet werden. Für die langsamen Stofftransportwellen, welche das Leistungsvermögen regenerativer Entfeuchter bestimmen, ergeben sich nur kleine Änderungen in der Nusselt- und Sherwood-Zahl. Das Separationsverfahren erweist sich als gut geeignetes Hilfsmittel zur Untersuchung experimentell bestimmter Ausgleichskurven.

НЕСТАЦИОНАРНЫЙ ТЕПЛО- И МАССОПЕРЕНОС ПРИ ЛАМИНАРНОМ ВЫНУЖДЕННОКОНВЕКТИВНОМ ТЕЧЕНИИ В КАНАЛАХ

Аннотация—При моделировании регенеративных тепло- и массообменников часто предполагается, что коэффициенты тепло- и массопереноса являются постоянными в различные моменты времени и в различных точках регенератора. В данной работе исследуется правомерность этого предположения. С использованием метода разделения изучаются экспериментальные кривые продувок опытного устройства с однократным продувом и матричным регенеративным осушителем. Кривые отклика заложены в модель, позволяющую рассчитывать временные и пространственные распределения коэффициентов тепло- и массопередачи к воздуху. Найдено, что числа Нуссельта и Шервуда изменяются незначительно для более медленных массопереносных волн, которые являются определяющими для работы регенеративных осушителей. Метод разделения оказал свою эффективность для анализа экспериментальных кривых продувок.